Measurement of contact stresses using real-time shearing interferometry

Liming Xu
Hareesh V. Tippur
Carl-Ernst Rousseau
Auburn University
Department of Mechanical Engineering
Auburn, Alabama 36849

Abstract. The optical method coherent gradient sensing, a real-time lateral shearing interferometry, is proposed for measuring contact stress fields under static and dynamic loading conditions. Feasibility of the method is first established under quasi-static conditions. Under dynamic conditions, the method has been used in conjunction with high-speed photography. The interference patterns representing stress gradients are used for extracting impact load history. Loading rates of approximately 14 MN/sec have been observed. The optical measurements are compared with the computed values obtained using finite element simulations.
[S0091-3286(99)01811-5]

Subject terms: shearing interferometry; coherent gradient sensing; contact stresses; dynamic loading; high-speed photography.

Paper 990032 received Jan. 25, 1999; revised manuscript received May 14, 1999; accepted for publication May 14, 1999.

1 Introduction

In view of simplicity of implementation and relative insensitivity to rigid body motions, real-time shearing interferometry has become a tool for a number of engineering investigations,[1–5] namely, optical component testing, experimental stress and strain analysis, and flame diagnostics. The underlying concept of the method involves quantification of the object wave front warping by measuring in-plane derivatives representing local angular deflections of light rays in the direction of shearing. This is accomplished through directional shearing of the object wave front using a variety of optical devices—prisms, gratings, or optical flats, to name a few. Recently, a lateral shearing interferometer with an on-line spatial filtering arrangement called coherent gradient sensing (CGS) has been proposed for photomechanics investigations.[3,4] The method is applicable to the study of both transparent and opaque objects. In the former, the warping of the object wave front is due to a combination of elasto-optic and Poisson effects, while in the latter it is due to the Poisson effect alone. The method has been used successfully in a number of static and dynamic fracture mechanics studies.

Mechanical response of materials subjected to impact loading is of practical significance in various engineering situations.[6] Some common examples include particle impact on airplane skin and coated turbine blades, missile impact on armor, manufacturing processes such as forging and high-speed machining, and other situations involving mechanical contact. The inertial and stress concentration effects in these situations often produce material damage. Some of the previous investigators have successfully demonstrated the applicability of optical techniques such as moiré photography,[7] digital speckle pattern interferometry,[8] and laser speckle interferometry[9] for mapping both in-plane and out-of-plane motion in solids subjected to impact loading. In the current study, CGS is used to study static and dynamic contact stress fields in a planar solid subjected to edge loading. The measurements are compared with idealized analytical and numerical models.

2 The Optical Technique

The optical arrangement for the method of coherent gradient sensing is shown in Fig. 1. A beam of laser light (wave length λ) is expanded and collimated. The light beam is transmitted through a transparent object or reflected from a specularly reflective opaque object. The object wave front is transmitted through a pair of Ronchi gratings G_1 and G_2 of pitch p with principal grating direction, say, parallel to the y axis. The separation distance between the two gratings along the optical axis is Δ. The resulting diffracted light emerging from the first grating consists of a zero and several odd diffraction orders. For the sake of simplicity and without losing generality, consider diffraction orders E_i $(i=0,\pm 1)$. Let $\theta_d[=\sin^{-1}(\lambda/p)]$ be the diffraction angle. Each of these diffracted wave fronts undergo a second diffraction and the wave fronts propagate in several discrete directions denoted by $E_{(i,j)}$ $(i=0,\pm 1,\ j=0,\pm 1)$. These are collected by a filtering/imaging lens and the spectral contents appear as a series of diffraction spots on the back focal plane of the lens. Using a filtering aperture, all but ± 1 diffraction orders are blocked as shown. The filtered information produces laterally sheared object wave fronts on the image plane resulting in a generic point Q on the object plane imaged at Q',Q'' on the image plane. Note that the imaging system is focused on the object plane.

Consider the interference produced in the overlapping portion of the sheared wave fronts on the image plane. For an undeformed specimen (or planar object wave front) [see Fig. 2(a)] the interference is due to the optical path difference between E_0 and $E_{\pm 1}$. The corresponding distribution of intensity on the image plane is governed by

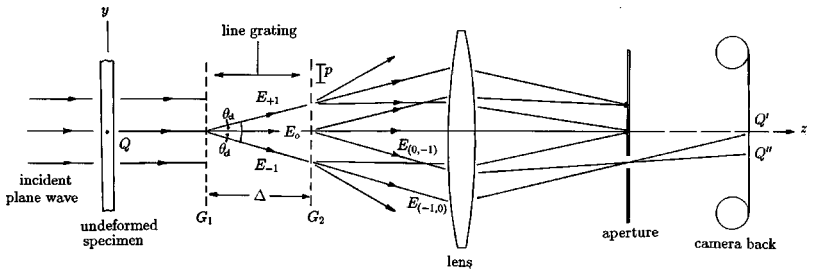

Fig. 1 Schematic of the optical setup and the working principle of coherent gradient sensing method.

$$I=(E_0+E_{\pm 1})(E_0+E_{\pm 1})^* \\ =A_0^2+A_1^2+2A_0A_1\cos k(l_0-l_1) \quad (1)$$

where A_0 and A_1 are maximum amplitudes, l_0 and l_1 are the geometric lengths associated with E_0 and $E_{\pm 1}$, respectively, and k is the wave number. The path difference (l_0-l_1) can be expressed as

$$(l_0-l_1)=\Delta(1-\cos\theta_d)\approx\Delta(\theta_d^2/2) \quad (2)$$

by expanding $\cos\theta_d$ in the neighborhood of zero and neglecting $O(\theta_d^3)$ terms compared to $O(\theta_d^2)$ terms. Then for constructive interference, $k(l_0-l_1)=2N\pi$ where $N=0, \pm 1, \pm 2, \ldots$, and hence, constructive interference occurs when

$$\theta_d/2=Np/\Delta \quad (3)$$

where $\theta_d=\lambda/p$ is used. When the object deforms, the incident plane wave front is perturbed due to non-uniform changes in thickness and/or refractive index of the specimen. Let the perturbed wave front propagate such that it makes an angle ϕ with the optical axis [see Fig. 2(b)]. The intensity distribution on the image plane is

$$I'=A_0^2+A_1^2+2A_0A_1\cos k(l_0'-l_1') \quad (4)$$

with $(l_0'-l_1')$ being the path lengths of E_0 and E_1 for the deformed specimen and

$$(l_0'-l_1')=\Delta\{(\cos\phi)^{-1}-[\cos(\theta_d-\phi)]^{-1}\} \\ \approx\Delta(-\theta_d\phi+\theta_d^2/2) \quad (5)$$

where terms smaller than ϕ^2, θ_d^2, and $\theta_d\phi$ are neglected. Again, for constructive interference

$$k\theta_d(\theta_d/2-\phi)=2N'\pi, \quad N=0,\pm 1,\pm 2,\ldots, \quad (6)$$

or

$$(\theta_d/2-\phi)=N'p/\Delta. \quad (7)$$

Now, one can express the propagation vector of the object wave front using its direction cosines, $\mathbf{d}=\alpha\mathbf{e}_x+\beta\mathbf{e}_y+\gamma\mathbf{e}_z$, where α, β, and γ are the direction cosines and $\mathbf{e}_x$, $\mathbf{e}_y$, and $\mathbf{e}_z$ are unit normal in the x, y, or z direction, respectively. For the case of in-plane deflection of light, $\alpha=0$, $\beta=\sin\phi$, and $\gamma=\cos\phi$. For small angles, $\beta\approx\phi$. Hence, using Eq. (3), Eq. (7) can be rewritten as

$$\beta\approx\phi=(N-N')p/\Delta\equiv np/\Delta \quad (8)$$

where $n=N-N'$. Thus, the interference patterns due to a deformed surface correspond to angular deflections corresponding to contours of constant β. For the case of a non-uniform spatial deformation relative to an initially flat surface, β changes from point-to-point and the fringes represent the deviations from the initial planarity of the object wave front. If the Ronchi gratings are oriented such that the principal direction is along the x axis, the measured fringes represent contours of constant α.

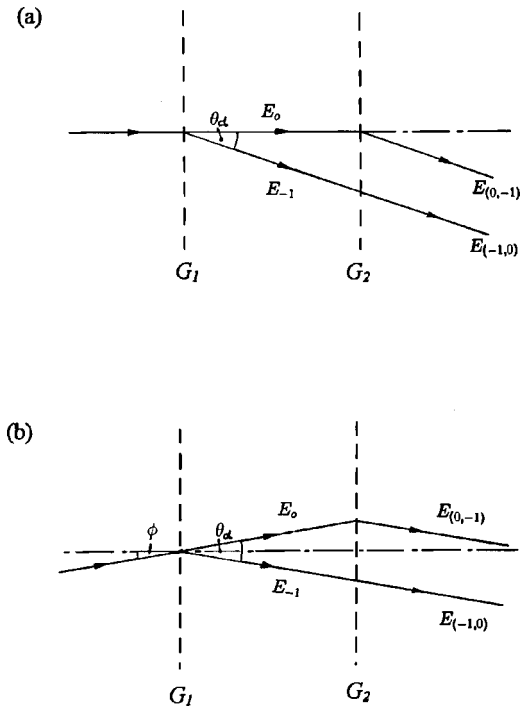

Fig. 2 Schematic of the diffracted wave for (a) an undeformed object and (b) a deformed object.

3 Interference Fringes and Deformation

For isotropic solids, non-uniform thickness and/or refractive index changes caused by the mechanical loads allow expression of the propagation vector as

$$\mathbf{d}=\frac{\partial(\delta S)}{\partial x}\mathbf{e}_x+\frac{\partial(\delta S)}{\partial y}\mathbf{e}_y+\mathbf{e}_z \tag{9}$$

where optical path length change δS can be related to stresses[4] under plane stress situation as

$$\delta S=cB(\sigma_x+\sigma_y)$$

where $c=c_t$ is an elasto-optic constant in transmission mode, $c=c_r$ is an elastic constant in the reflection mode, and B is the nominal thickness of the planar object. The governing equation for transmission mode is,[4]

$$c_tB\frac{\partial(\sigma_x+\sigma_y)}{\partial x(\text{or }\ \partial y)}=\frac{np}{\Delta},\quad n=0,\pm1,\pm2,\ldots, \tag{10}$$

and for reflection mode is

$$2\frac{\partial w}{\partial x(\text{or }\ \partial y)}=c_rB\frac{\partial(\sigma_x+\sigma_y)}{\partial x(\text{or }\ \partial y)}=\frac{np}{\Delta},\quad n=0,\pm1,\pm2,\ldots, \tag{11}$$

where w is the out-of-plane displacement of the object surface.

4 Line Load Acting on a Planar Half-Space: Static Loading

The problem of stress amplification between contacting elements is an important engineering problem. In our study, application of shearing interferometry to map two-dimensional stress fields in a transparent model under static loading conditions was undertaken first. A polymethylmethacrylate (PMMA) sheet of nominal thickness of 9 mm was subjected to a line load using a cylindrical profile steel loading fixture. Before applying the load, a uniform bright field was obtained in the region of interest. The fringe pattern near the vicinity of the edge load is shown in Fig. 3(a) for a load level of approximately 1500 N. Other experimental parameters used in the experiment were grating pitch $p=25.4\ \mu$m, grating separation distance $\Delta=38$ mm, and wave length of light $\lambda=633$ nm. The resulting optical sensitivity is approximately 6.6×10^{-4} rad/fringe. The profile of the contacting cylinder is also clearly visible in the figure. The far field region is essentially a uniform bright field $(n=0)$ while the contact region has an intense concentration of fringes that are symmetric about the loading axis representing stress amplification. As one approaches the contact point, the angular deflection of light increases and the finite dimension of the filtering aperture blocks the information very close to the contact point and, hence, loss of some optical information occurs.

A closed form elastic solution for the problem exists in the literature[5] with the hydrostatic stress for plane stress given by

$$(\sigma_x+\sigma_y)=-\frac{2P\cos\theta}{\pi Br} \tag{12}$$

where (r,θ) are the polar coordinates as shown in Fig. 3(b), and P is the applied load. It can be seen that the stresses

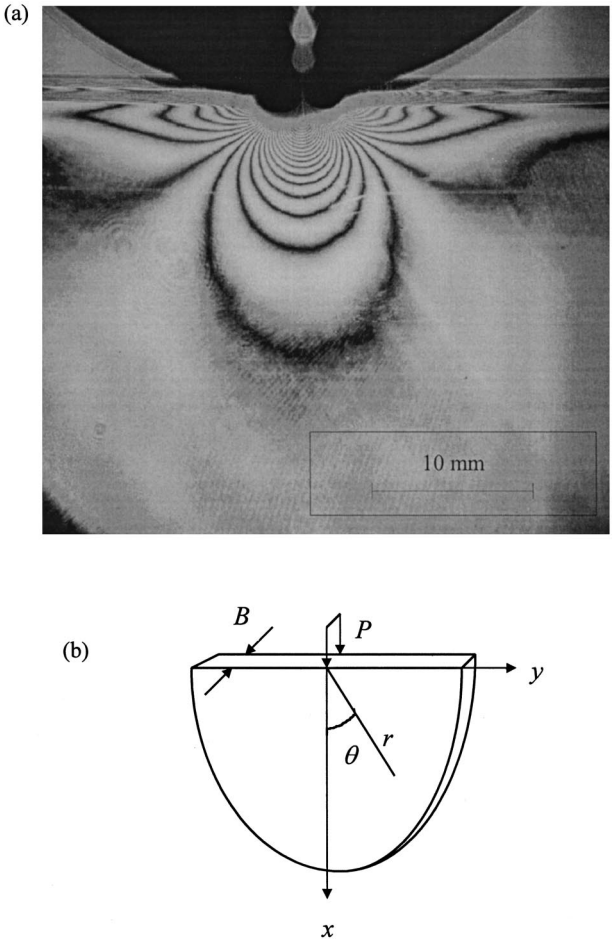

Fig. 3 (a) CGS fringes representing contours of $(\sigma_x+\sigma_y)$ gradients in the x direction for a statically loaded PMMA sheet, and (b) schematic of line load acting on the edge of a planar object.

tend to infinity as $r\to0$, suggesting a singular behavior near the applied load. For the field quantity under consideration, the relationship between the idealized mechanical field and the interference fringes becomes

$$c_t\frac{2P\cos2\theta}{\pi r^2}=\frac{np}{\Delta}. \tag{13}$$

For PMMA the elasto-optic constant is $c_t\cong-0.9$ m^2/N.[10] From this, one can estimate the applied load P using optical interference data, and measurements along $\theta=0°$ are plotted in Fig. 4 as solid symbols while the broken line represents the applied load measured using a load cell. The optical measurements are in good agreement with the applied load over a range of normalized radial distance of $0.4<r/B<1.2$. As one approaches the point of application of the load, the optical measurements underestimate the actual value due to (a) the break down of the planar assumptions near the stress concentration, (b) finite area of contact resulting from deformations, and/or (c) material nonlinearity effects. Also, as one moves sufficiently far away from the point of application of the load, say, beyond $r/B\sim1.2$, the far field state of stress that is ignored in Eq. (12) begins to affect the description.

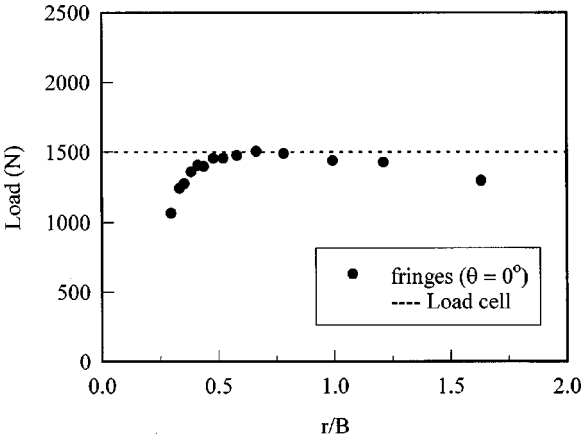

Fig. 4 Comparison of optically measured load from the CGS fringes with the applied load.

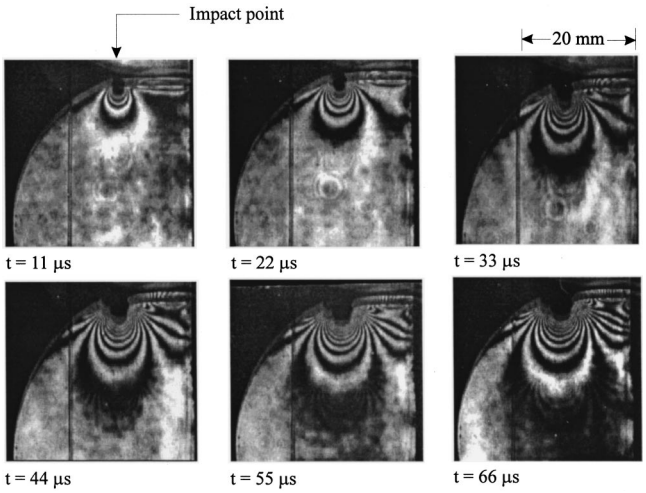

Fig. 6 Representative fringe patterns near the vicinity of the impact load acting on the edge of the PMMA sheet near a polymer-metal interface.

5 Line Load Acting on a Planar Sheet: Dynamic Loading

Next, mapping of contact stress fields during impact loading using real-time shearing interferometry was undertaken. The evolution of dynamic stress fields in a PMMA sample was recorded using CGS optical setup in conjunction with high-speed photography. The schematic of the experimental setup is shown in Fig. 5. It consisted of a cavity dumped argon-ion laser operating at a 514-nm wave length as a coherent strobe light. The rest of the optical setup was similar to the one used in the quasi-static investigation with grating separation distance $\Delta = 70$ mm. The interference patterns were captured using a rotating mirror high-speed camera. A framing rate of 185,000 fps with individual frames exposed over a 50-ns duration was used during the experiment. A co-axially mounted three-facet mirror attached to a compressed air driven turbine shaft swept the image onto a stationary 35-mm film (400 ASA T-Max) held in a circular arc over 240°.

The test sample consisted of a PMMA sheet of dimensions $150 \times 50 \times 6$ mm bonded to an aluminum sheet of same dimensions along a 50×6 mm surface. The sample was supported between two anvils 280 mm apart relative to the load line. The sample was impacted on the PMMA edge at a distance of 12.5 mm from the bond line by launching a pneumatically operated linear thruster. The impact was delivered through a steel tup (approximate weight 7.5 kg) attached to the actuator with an impact velocity of approximately 3.5 m/s. A thin (~ 100 μm) adhesive back copper film was fixed to the PMMA edge in the contact region and was made part of a laser triggering circuit. First the rotating mirror was brought to the required speed prior to launching the impactor. The impactor, upon contacting the specimen (time $t = 0$ sec), triggered the laser to produce a string of laser pulses at the preset repetition rate over a gated period lasting a third of the period of the turbine shaft rotation. The resulting interference fringes were captured on the film.

A few representative fringe patterns from the early stages of the impact from $t = 0$ to 66 μs are shown in Fig. 6. The fringe sensitivity is 3.6×10^{-4} rad/fringe. It should be noted that the far field essentially remains a uniform light fringe ($n = 0$) over the period under consideration.

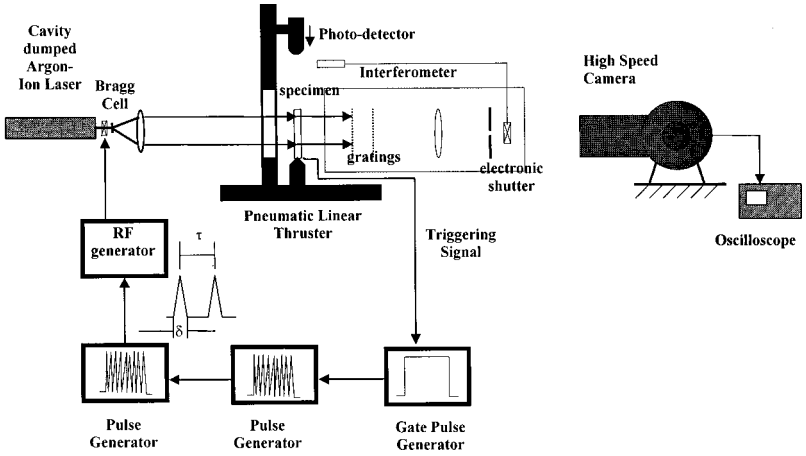

Fig. 5 Schematic of the experimental setup used for dynamic contact stress field mapping using CGS and high-speed photography.

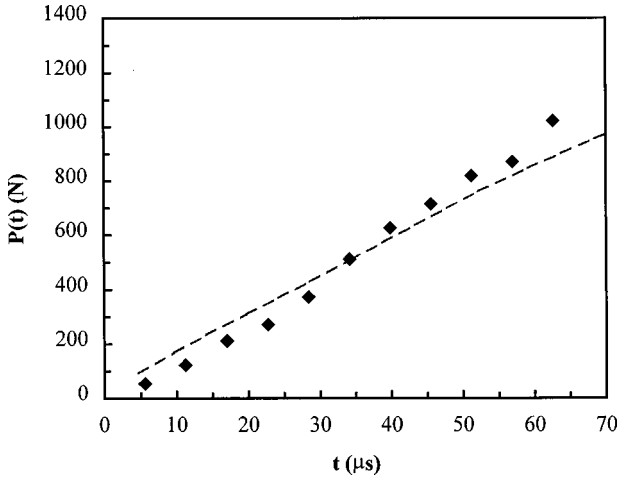

Fig. 7 The loading history obtained from the CGS fringes (solid symbols) and finite element simulation (broken line) based on constant velocity impact on PMMA.

Evidently, the fringe patterns resemble the ones obtained during static experiments. This suggests that the stress field equations for the dynamic stresses are similar to the ones in Eq. (13) and all the inertial effects due to dynamic loading enter through the instantaneous load level $P=P(t)$. Thus, using a procedure identical to the one used for analyzing the static fringe patterns, the loading history $P(t)$ was obtained. The loading history thus obtained is plotted in Fig. 7 and each value is an average of the ones obtained by considering fringe data in the region $0.5<r/B<1.0$ in the analysis along $\theta=0°$. The loading history seems to be essentially linear, suggesting a ramp loading with a loading rate of approximately 14 MN/s over the duration.

The measurements thus obtained need to be independently validated since there is no closed form solution available for comparing the experimental data in this case. Hence, a finite element simulation of the impact experiment was undertaken. The simulation was carried out using an ANSYS™ finite element package. The plane stress elasto-

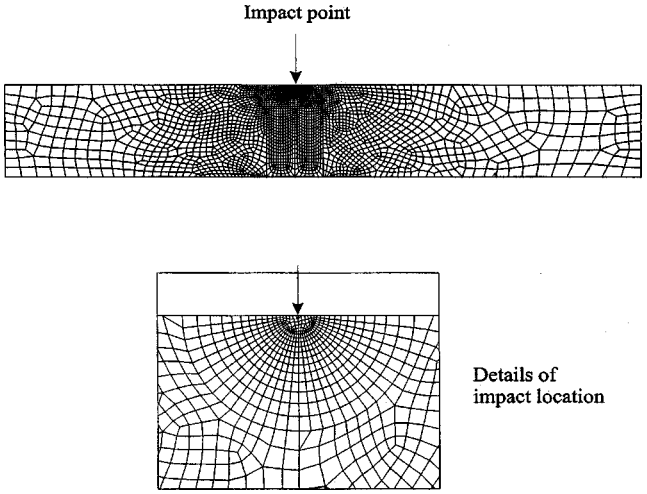

Fig. 8 Finite element discretization of the model used in the computations.

Table 1 Dynamic material properties.

	Young's modulus (GPa)	Poisson's ratio	Longitudinal wave speed (m/s)	Shear wave speed (m/s)
PMMA	3.3	0.35	2080	1000
Aluminum	70.0	0.30	6300	3100
Steel	200.0	0.28	5900	3200

dynamic finite element model [see Fig. 8] consisted of 2826 eight-node isoparametric elements subjected to constant velocity line loading of 3.5 m/s. The assumption of constant tup velocity during the impact is reasonable in view of the large modulus ratio between the tup/impactor and PMMA [see Table 1]. The computed values of the impact load are shown in Fig. 7 as a broken line. Evidently, the agreement between the two results is good over the duration. The experimental results overestimate the load level toward the end of the duration due to the interaction between the metal interface and the loading point that is not considered in the analysis of the experimental results.

6 Conclusions

The method of real-time shearing interferometry has been extended for stress field examination in the vicinity of a cylindrical contact at the edge of a planar half-space. The stress fields have been mapped under both static and low velocity loading conditions. High-speed photography is used to record interference fringes for the case of a constant velocity impact on the edge of a PMMA sheet. The dynamic loading history has been directly evaluated by interpreting the fringe data through stress field equations for a homogeneous half-space. In view of the closeness of the impact point to interface between the polymer and the metal, independent elasto-dynamic finite element simulations were undertaken. The computed values of the instantaneous load at the contact point are seen to be in good agreement with the optical measurements.

References

1. K. Patorski, ''Shearing interferometry and the moiré method for shear strain determination,'' *Appl. Opt.* **25**, 3567–3572 (1988).
2. K. Patorski, S. Yokozeki, and T. Suzuki, ''Collimation test by double grating shearing interferometer,'' *Appl. Opt.* **15**, 1234–1240 (1972).
3. H. V. Tippur, ''Coherent gradient sensing: a Fourier optics analysis and application to fracture,'' *Appl. Opt.* **31**(22), 4428–4439 (1992).
4. H. V. Tippur and A. J. Rosakis, ''Quasi-static and dynamic crack growth along bimaterial interfaces: a note on crack tip field measurements,'' *Exp. Mech.* **31**, 243–251 (1991).
5. H. Philipp, H. Fuchs, and E. Winklhofer, ''Flame diagnostics by light sheet imaging and by shearing interferometry,'' *Opt. Eng.* **32**(5), 1025–1032 (1993).
6. L. Johnson, *Contact Mechanics*, Cambridge University Press (1998).
7. M. Huntley and J. E. Field, ''High resolution moiré photography: application dynamic stress analysis,'' *Opt. Eng.* **28**(8), 926–932 (1989).
8. J. Tong, D. Zhang, H. Li, and L. Li, ''Study on in-plane displacement measurement under impact loading using digital speckle pattern interferometry,'' *Opt. Eng.* **35**(4), 1080–1083 (1996).
9. B. W. Asay, G. W. Laabs, B. F. Henson, and D. J. Funk, ''Speckle photography during dynamic impact of an energetic material using laser fluorescence,'' *J. Appl. Phys.* **82**(3), 1093–1099 (1997).
10. P. Ganeshan and H. V. Tippur, ''*Interferometric measurement of thermally induced interface crack tip stress fields*,'' *Proc. SEM Spring Conf.*, Baltimore, MD, pp. 218–223 (1994).

Liming Xu obtained BS and MS degrees in civil engineering from Northern Jiaotong University in 1983 and 1986, respectively. He worked as a senior research engineer until 1991 at the Institute of Engineering Mechanics in Beijing before coming to the U.S. to pursue a doctoral degree. He received a PhD in mechanical engineering from Auburn University in 1996. Currently, he is with GE Power Systems in Schenectedy, New York. His interests include fracture mechanics, experimental mechanics, stress analysis, and solid modeling.

Hareesh V. Tippur obtained MS and PhD degrees from Indian Institute of Science and State University of New York at Stony Brook in 1982 and 1988, respectively. He was a postdoctoral fellow at California Institute of Technology before joining Auburn University in 1990. Currently, he is an associate professor and leads the failure characterization and optical techniques lab at Auburn. He has worked extensively in the area of optical techniques for failure characterization. His work has resulted in combined moiré and laser speckle techniques for simultaneous measurement of all three displacement components near cracks and a new shearing interferometry called coherent gradient sensing for static and dynamic fracture mechanics studies. He has received the Hetenyi award from the Society of Experimental Mechanics for outstanding research publication in *Experimental Mechanics* and has been recognized as an outstanding new mechanics educator by the American Society for Engineering Education. His current interdisciplinary interests include visible and infrared techniques for metrology, interfacial fracture mechanics, and failure characterization of functionally graded materials.

Carl-Ernst Rousseau obtained his BS and MS degrees in mechanical engineering from the University of Florida. Upon graduation in 1989, he went to work for Westinghouse Electric Corporation, designing and performing stress analysis of components of nuclear power plants. Since 1997, he has been pursuing a PhD in mechanical engineering, focusing on fracture mechanics of functionally graded materials. His current interests include the application of optical and numerical techniques to failure characterization of materials.